Asian Journal of Geological Research

4(3): 16-36, 2021; Article no.AJOGER.69750

Geological and Geochemical Characterisation of Fe-Mn Oxide Mineralisation of Wadi Masilah Basin (SE Yemen)

Laura Pinarelli[1*] and Mohammed A. Mattash[2]

[1]Institute of Geosciences and Earth Resources, National Research Council (CNR), Florence, Italy.
[2]Geological Survey and Minerals Resources Board, Sanaa, Yemen.

Authors' contributions

This work was carried out in collaboration between both authors. Both authors read and approved the final manuscript.

Article Information

Editor(s):
(1) Dr. Ahmed Abdelraheem Frghaly, Sohag University, Egypt.
Reviewers:
(1) Amany. H. K .Said, China University of Petroleum Beijing, China and Assiut University, Egypt.
(2) Usha Chirala, Andhra University, India.
Complete Peer review History: http://www.sdiarticle4.com/review-history/69750

Original Research Article

Received 10 April 2021
Accepted 15 June 2021
Published 16 June 2021

ABSTRACT

The Wadi Masilah Basin is part of the larger Say'un-Masilah Basin, a Mesozoic sedimentary basin located in the southeastern Yemen. It consists of a sedimentary sequence hosting polymetallic barite, lead, zinc, iron, manganese, and vanadium mineralisations. The area is strongly faulted as a result of extensional and transtensional tectonics connected to the opening of the Gulf of Aden-Red Sea rift system. Quaternary volcanic activity is associated to the post-rift phase. The present paper deals with the Fe-Mn oxide mineralisation hosted by Cretaceous and Eocenic shallow marine carbonates. The mineralogical assemblage consists of hematite, limonite, goethite, hollandite, romanechite, cryptomelane, pyrolusite, and rodochrosite. Mineralisation may be stockwork, vein-like, and disseminated in carbonate rocks. Iron orebodies made up of massive hematite contain ~80-74% Fe_2O_3. Mineralised veins have tenors of Fe_2O_3 variable from ~ 52% to ~11%. Pb, Cr, and Zn contents can be high in some samples. Manganese orebodies have mostly high MnO tenors (~65-52%) and are characterised by very high Ba, Pb, and Zn contents. The disseminated carbonate rocks have Fe_2O_3 contents up to ~13%, and MnO contents up to ~5%. Their Pb and Zn contents can locally be very high. Samples coming from 12 drillcores, mostly limestones and dolomitic limestones are low-grade in both Fe_2O_3 (~6-0.4%) and MnO (~0.8-0.1%).

**Corresponding author: Email: laura.pinarelli@gmail.com;*

As for the source of the mineralising fluids, discriminative diagrams based on Fe/Mn and transition metals support a hydrothermal origin with possible contribution from diagenetic processes. The distribution of Zn and HFSE suggests that hydrothermal mineralising fluids are related to the magmatic-hydrothermal systems affiliated to the neighbouring Quaternary volcanic fields. Widespread positive Ce spikes in the trace element patterns suggest the Fe-Mn ore deposition occurred in a relatively shallow, oxidizing environment.

Keywords: Geochemical characterisation; Fe-Mn oxide; mineralisation; oxidizing environment.

1. INTRODUCTION

The Republic of Yemen forms the southwestern tip of the Arabian Peninsula and overlooks the Arabian Sea, the Gulf of Aden, and the Red Sea, with 1,906 km of coastline. Yemen's economy was largely dependent on revenue from the export of hydrocarbons, however Yemeni terrain is also enriched in both metallic and nonmetallic commodities, including base metals, precious metals, as well as a variety of industrial materials and dimension stones. Despite most of the exploration of the last decades has been focusing on hydrocarbons and natural gas, several mining licenses have been active in Yemen [1,2], including, but not limited to, the Governorate of Sana (copper, gold, iron, lead, silver and zinc), the Governorate of Dhale (iron and associated minerals), the Governorate of Taizz (chromium, copper, gold, iron, nickel, and silver), the Governorate of Hajjah (gold and associated minerals), and the Governorate of Marib (iron ore and associated minerals).

The Wadi Masilah Basin, located in the Governorate of Al-Mahrah in southeastern Yemen, hosts a number of important barite, lead, zinc, iron, manganese, and vanadium mineralizations.

An overview of the mineral resources available in the Wadi Masilah Basin can be found in [3]. These occurrences have been investigated with extensive fieldwork since many years by one of the present authors (M.M.) and his geologic group as part of the Geological Survey and Minerals Resources Board of Sanaa [4-7].

On account of the security issues caused by civil strife and political uncertainty, the mineral sector in Yemen had a slow progress. Characterising Fe-Mn oxide mineralization may be important to attract foreign as well as local companies to operate in the country. The objective of the present paper is providing a better understanding of the Fe-Mn mineralization processes and characterizing the origin of the mineralising fluids based on geological and geochemical features.

2. GEOLOGICAL SETTING

2.1 Regional Geology

Yemen is situated in the southwestern part of the Arabian Peninsula (Fig. 1, inset), and its basement complex is part of the Arabian Shield, within the larger framework of the Arabian-Nubian Shield. The stratigraphy and regional geology of Yemen was established by detailed works [e.g.8,9]. Hydrocarbon exploration activity after the '90s allowed for a revised synthesis of basin evolution in Yemen, such as the work of [10-13].

The Precambrian basement rocks in Yemen comprise metavolcanic, metasedimentary, gneiss and migmatitic belts produced in arc environments intruded by post tectonic granites and granodiorites. The oldest known rocks occur in the Al Bayda terrane, which contains late Archaean aged (Sm-Nd: 2700-2900 Ma) gneisses, amphibolite dykes and granites. Over the basement rocks, twelve sedimentary basins were identified (Fig. 1), categorised into three groups according to their age: Palaeozoic, Mesozoic and Cenozoic [14] and references therein]. The geological evolution of Yemen was driven by two main tectonic events: (i) the Late Jurassic rifting between east Africa and west India that caused extensional tectonics. The dominant feature was the generation of horst/graben structures that shaped new topographies for sediment accumulation, without any volcanic activity; (ii) the opening of the Gulf of Aden-Red Sea rift system that started the separation of the Arabian Peninsula from Africa. The rifting, that began in the Oligocene and is still active, was associated to the emplacement of large volumes of flood basalts [15]. Extensional tectonics resulted in rift shoulder uplift (exposing the Precambrian basement in western Yemen), basin subsidence, and sediment filling with a thick succession from

fluvial/coastal through shallow marine to deep marine facies. Subsequently, Plio-Quaternary volcanic rocks were emplaced in four major volcanic fields, Sana'a-Amran, Dhamar-Rada'a, Marib-Sirwah and Balhaf–Bir Ali, which compose the Aden volcanic line [16].

2.2 Geology of Wadi Masilah Basin

The Wadi Masilah Basin **(**WMB) is located in Al-Mahrah Governorate whose capital and largest city is the port Al Gahyda, approximately between 485000-510500E and 1688500-1720200N, UTM coordinates. The Al-Mahrah Governorate is crossed by a very sparse network of deeply cut wadis (seasonal watercourses), the biggest one of which is the dry and inhospitable Wadi Masilah that flows into the sea near the city of Seyhoot.

The WMB belongs to the Masilah Sector of the Say'un-Masilah Basin (Fig. 1), a basin developed in Late Jurassic to Early Cretaceous times. The geological map of the WMB is reported in Fig. 2.

The stratigraphic succession in the WMB starts with the Amran group, composed by Jurassic dolomitised carbonates of the Shuqra Formation, followed by marine sediments of the Madbi formation, characterized by more open marine pelagic carbonate facies with marls and claystones. This facies continues upwards in the overlying Nayfa Formation. Carbonate deposition of the Nayfa Formation continued across the Jurassic-Cretaceous time boundary with shales, carbonates and clastics of the Saa'r Formation following the Nayfa without any apparent break in the gorge of the WMB. The Saa'r Formation is unconformably overlaid by the Qishn Formation, which constitutes the basal unit of the clastic-dominated Tawilah/Mahrah Group, marking a new transgression from the east. The succession starts with basal transgressive sands of the Harshiyat Formation, followed by

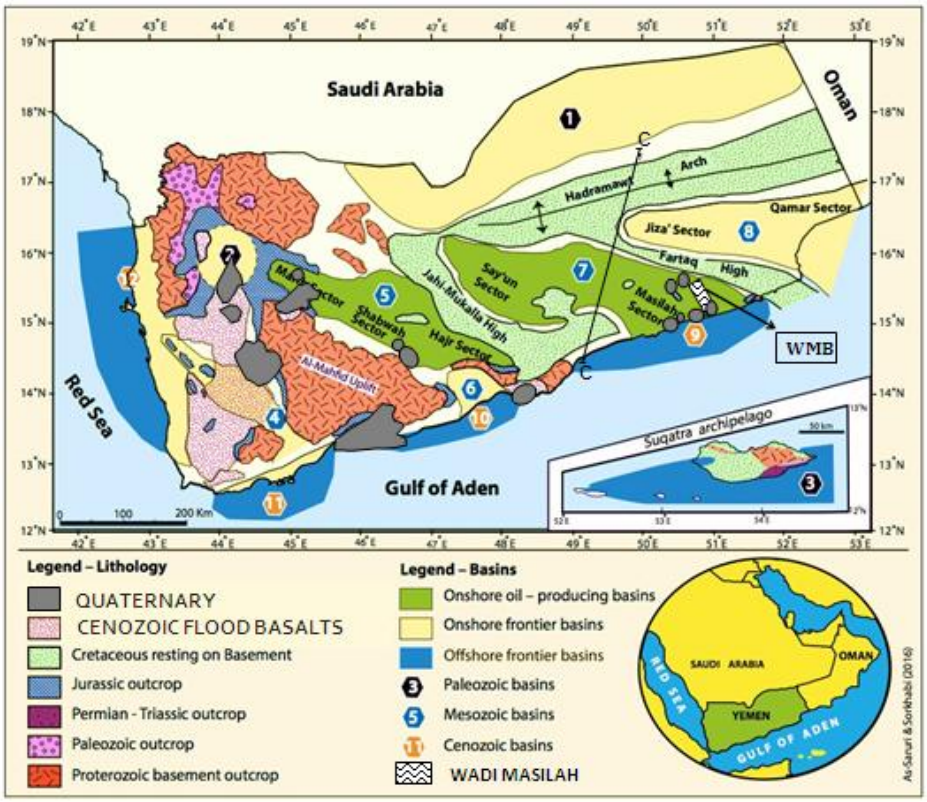

Fig. 1 Map of the outcropping geology, major structural highs, and sedimentary basins of Yemen, and location of the Wadi Masilah Basin (WMB). Modified after [14,17]. Location of Quaternary volcanic rocks after [18]

the clastic-dominated Mukalla Formation. Above are the Paleocene-Eocene rocks of Umm Er-Rhaduma Formation, constituted by interbedded light grey shales and marly limestones, and Jeza Formation, made up of thinly bedded dolomitic limestones. The region is overlaid by the Oligo-Miocenic Shihr Group deposits, originating from the erosion of Eocene rocks. This results in intercalations of variegated clay (red, dark brown, and pale green), sandstone, conglomerate, thin limestone beds, and gypsiferous layers. Several small areas are covered by Quaternary alkali olivine basalt lava flows, associated to the post-rift phase of the Red Sea and Gulf of Aden [19], which began in the northwestern area and extended to the southeastern part of the wadi. A very thin layer of Quaternary sediments occurs, consisting of partially cemented gravels, whereas the uppermost part is composed of a thin recent layer of soils and sands.

The WMB underwent complex structural events, including extensional and transtensional regimes, resulted, in general, from the syn- (late Oligocene-early Miocene) and post- (late Miocene-Recent) rift phases of the Red Sea and Gulf of Aden opening, with NW-SE and NE-SW major fault zones, respectively. As a result, the prospect area has been strongly faulted. Normal as well as thrust faults are characteristic features, whereas fissures and joints are common structural patterns. Small horsts and grabens are locally developed, indicating complex faulting activity. As well, some parts of the sedimentary sequence are slightly subjected to folding.

The WMB hosts a number of barite and associated base metal ores, namely barite-lead-zinc-iron-manganese-vanadium mineralisations. Economic minerals occur entirely in the residual sedimentary plateau composed by limestones, dolostones, and silicified limestones, which overlie the late Proterozoic basement in the southern part of WMB.

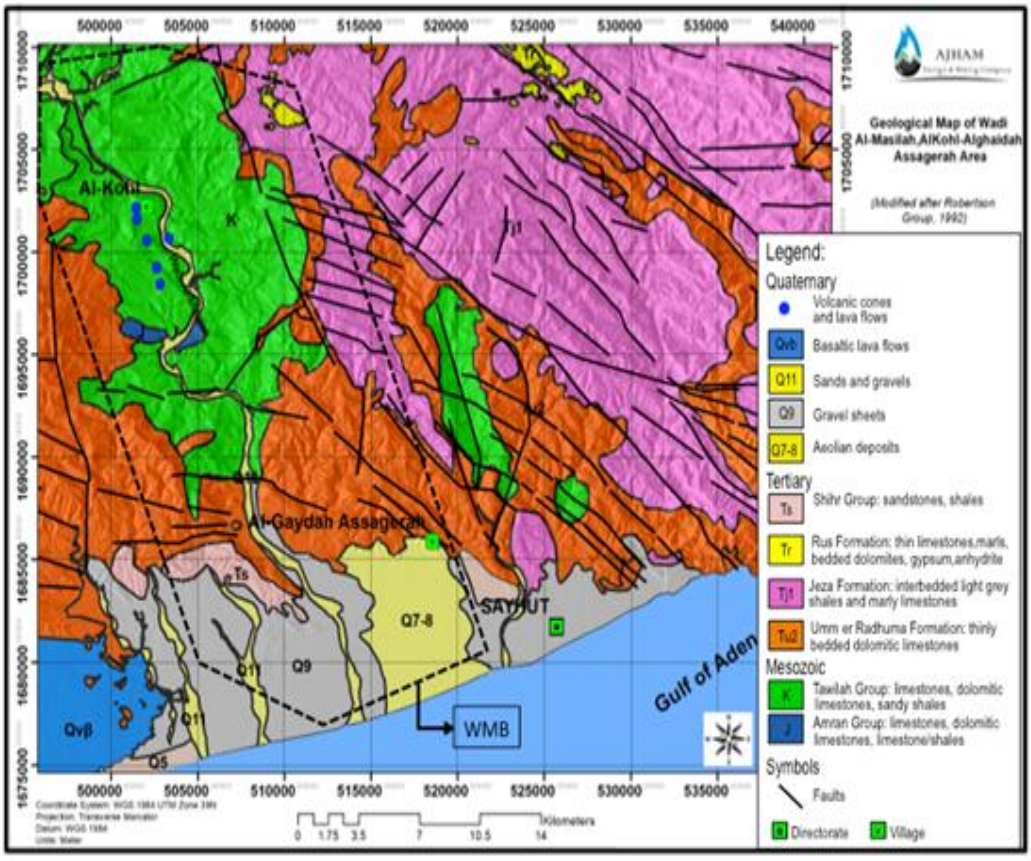

Fig. 2. Geological map illustrating the most important lithologic units and the major structural patterns of the WMB (dashed envelope)

2.3 Geometry and Structures of the Fe-Mn Oxide Deposits

The present paper deals with the Fe-Mn oxide mineralisation cropping out at Al-Kohl1, Al-Kohl2, and Al-Gaydah prospects (Fig. 2). At Al-Kohl1 and Al-Koh2 prospects the mineralisation is hosted by the Cretaceous carbonates of Tawilah Group (K in Fig.2), whereas at Al-Gaydah prospect the mineralisation is hosted by the Eocenic shallow marine carbonates associated with the base of Umm Er Radhuma Formation (Tu_2 in Fig.2). In addition, significant occurrence of manganese ore at a depth of 80 to 200 m was indicated by a geophysical survey carried out 25 km to the southeast of Al-Gaydah deposit (Fig. 3). Fossil records suggest that mineralisation started during Cretaceous time and continued up to Quaternary, in the post-rift phase of the Red Sea-Gulf of Aden rift system.

Three types of mineralisation were recognised in the WMB deposit, related to the geometry of the ore-bearing structures: stockwork, vein-like, and disseminated. Stockwork mineralisation is either structurally controlled or randomly oriented, the latter being dependent on the occurrence of brittle structures, cavities and vugs. Several discordant irregular veins striking NW-SE, and near horizontal, or in some cases steep dipping, orebodies, are present.

Vein-like orebodies occur both as massive veins several hundred meters long (max 1.5km) ranging in width from 1 m to few tens of meters (max 40m), and as smaller veinlets a few metres long ranging in width from some centimetres to 1m. Mineralisation style is either breccia-filling, or cavity and pore filling, often characterized by botryoidal texture. Patches, impregnations and disseminations are scattered throughout the host calcareous rocks.

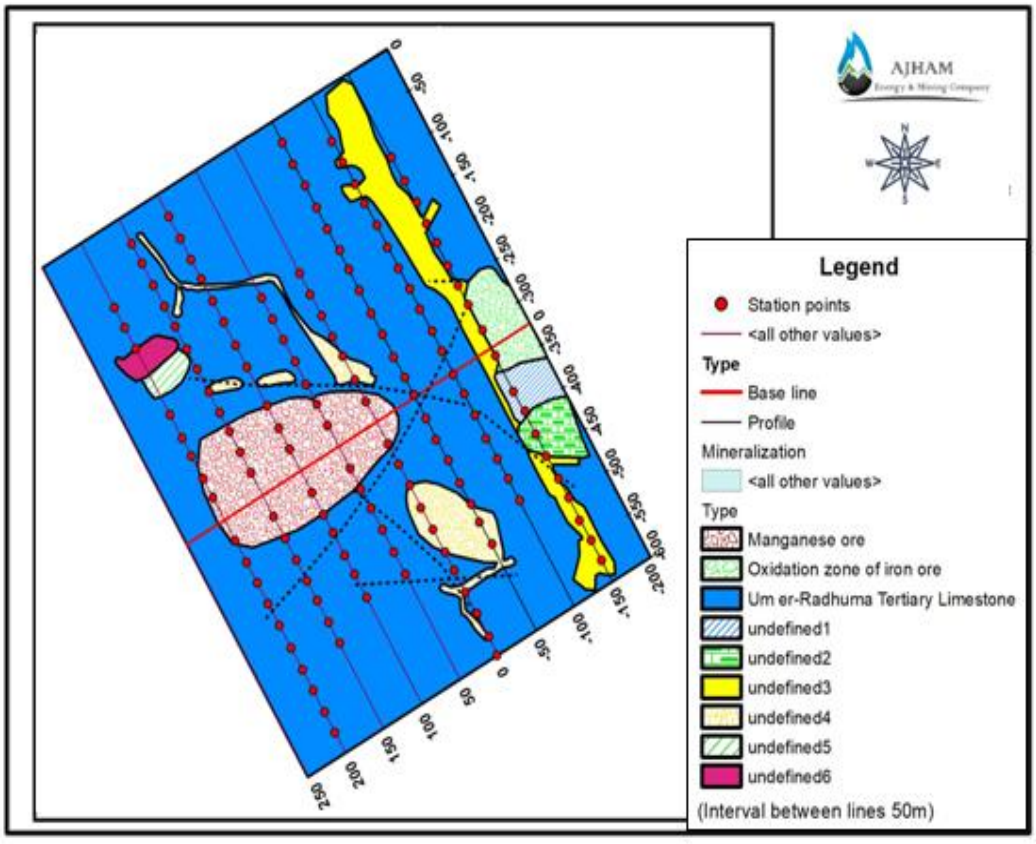

Fig. 3. Results of electromagnetic - induced polarization geophysical survey carried out at Algaidhah Assagirah, 25 km to the southeast of Al-Gaydah prospect. Derived imaging, obtained by forward method and inversion, indicates the occurrence of a manganese ore at a depth of 80 to 200 m below the surface

3. MATERIALS AND METHODS

The mineralogical and geochemical study was carried on selected samples, representative of the many outcrop samples collected during the fieldwork. Sixteen samples of Fe orebodies were collected from both massive Fe oxide and veins of polymetallic ores. Eight samples of Mn orebodies were taken from both massive Mn oxide and polymetallic veins and lenses. Fifteen samples of Fe-Mn disseminated carbonate rocks were taken from compact or brecciated carbonate rocks in the close proximity of mineralised veins and lenses. Eighteen samples of non-mineralised limestones and dolomitic limestones were taken from the country rocks of Alkhol1 and Alkhol2 prospects. In addition, 100 sections of 12 drillcores from the Alkohl1 drillings (Fig. 4), each one mostly ca.1m in length, were also analysed (geochemical data are given in Online Resource 1).

Before bulk rock geochemical analysis, samples were prepared at the geochemical laboratory of the Geological Survey and Minerals Resources of Hadramawt, with techniques including: (i) drying in forced air oven in stainless steel trays at 40°C for 48 hours; (ii) crushing in a jaw crusher for creating granular material of 1 mm from hand samples (iii) pulverising granular material in agate bowl to very fine grained powder.

Identification of mineralogical species was achieved by X-ray powder diffraction (XRD) analysis at the University of British Columbia (Canada) with Bruker AXS D8 Focus and D8 Advance X-ray powder diffractometers.

Whole rock chemical analyses of major, minor, and trace elements were carried out at als chemex laboratory, vancouver, canada. Different analytical methods were selected based on both type of rock/mineral and concentration of the elements to be detected. In particular, the chemical procedures of sample digestion were the aqua regia method and the four acid digestion methods. The instrumental methods of analysis were inductively coupled plasma atomic emission spectroscopy (icp-aes) and inductively coupled plasma mass spectrometry (icp-ms). The acronyms referred to

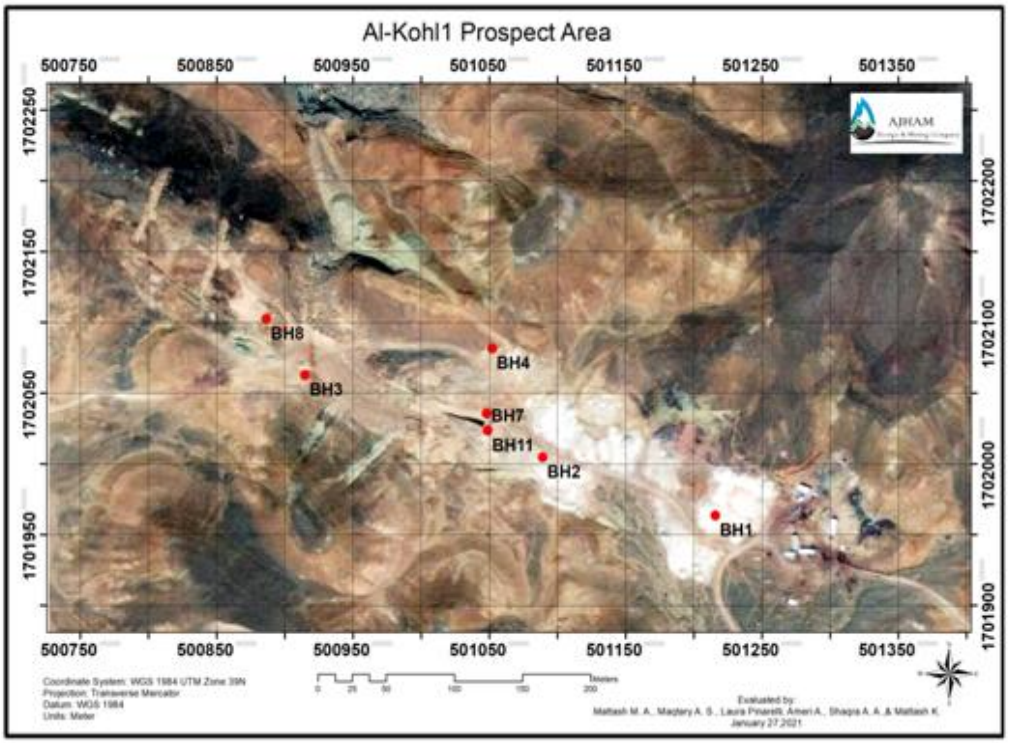

Fig. 4. Landsat image showing the location of the drilled exploratory wells performed in the Al-Kohl1 prospect area in limestone and dolostone of Saár Formation. White colour = barite

in the column "Analytical methods" of Table 3 represent different combinations of the above described chemical+instrumental procedures, as follows:

"ME-ICP41, OG46": Aqua regia digestion + ICP-AES. "ME-ICP61, OG62": Four acid digestion + ICP-AES. "ME-MS61": Four acid digestion + ICP-MS.

Additional details on the analytical methods and detection limits can be found in the site of ALS [20].

4. RESULTS

4.1. Occurrence and Mineralogy of Ores

According to XRD analyses, the mineralogical assemblage of the WMB Fe-Mn ore consists of hollandite, romanechite, cryptomelane, pyrolusite, rodochrosite, hematite, limonite, and goethite (Table 1). Mineralisation is either confined in veins and stockwork, or dispersed as disseminations and patches in the host calcareous rocks. Calcite is widespread, both as gangue mineral, and as lately recrystallized form, often in association with vein contacts. Euhedral coarse, medium and fine-grained quartz crystals occur as cavity or drusy filling. In addition, chalcedony and jasper occur as latest generation. Dolomitisation, limonitisation, and silicification are widespread in the prospects.

4.1.1. Iron ores

Hematite, goethite and limonite occur at the close vicinity of the manganese occurrences, in an intensively silicified material. Hematite may occur either in massive veins (Fig. 5a-b), attaining in some cases 40m in width and 300m in length, or in polymetallic hematite-galena, hematite-barite-galena, hematite-calcite-galena, and hematite-quartz veins. Hematite-barite and hematite-barite-silicified dolostone stockwork breccias are also present. Hematite has dark grey, reddish brown, red or black colour (Fig.5d, b, d). Sometimes, it forms thin six-sided platy crystals, and/or lens shaped scales. Limonite is found as pseudomorphous after hematite (Fig. 6e); it has yellow-brown and yellow colours, and usually forms botryoidal masses, sometimes earthy. Goethite occurs as cavity and pore filling, characterized by botryoidal structure (Fig. 5c). Iron oxides were also found either as patches on rosettes of barite and quartz (Fig. f), or as individual hematite-rich boulders.

Table 1. List of minerals occurring in the WMB Fe-Mn ores

Mineral	Ideal formula	Colour	Hardness	Specific Gravity
Hollandite	$Ba(Mn^{4+},Mn^{2+})_8O_{16}$	Black to steel grey	6	4.5-5.0
Romanechite	$(BaH_2O)_2(Mn^{4+},Mn^{3+})_5O_{10}$	Black to steel grey	6	4.7-5
Cryptomelane	KMn_8O_{16}	Black to steel grey	5-6	4.3
Pyrolusite	MnO_2	Steel grey to black	6-7	5
Rodochrosite	$MnCO_3$	Pink to rose-red	3.5-4	3.7
Hematite	Fe_2O_3	Metallic grey	5.5-6.5	5.3
Limonite	$FeO(OH)•nH_2O$	Various shades of brown and yellow	4-5.5	2.9-4.3
Goetite	□•FeO(OH)	Dark brown to black	5-5.5	3.3-4.3

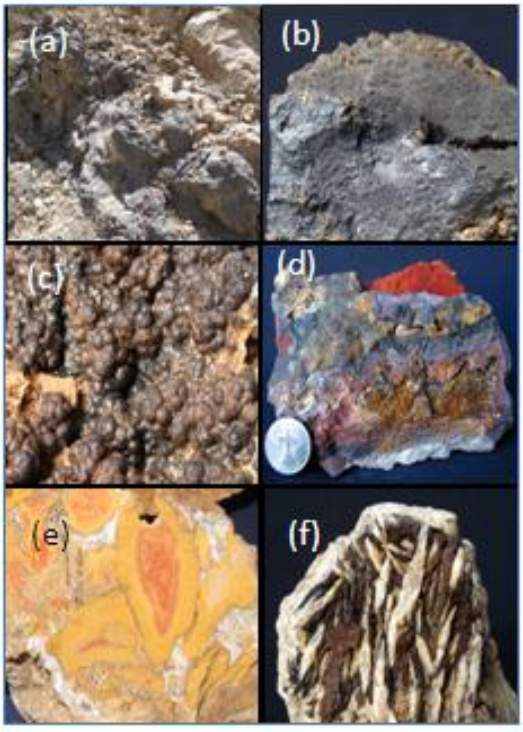

Fig. 5. Different structures and textures of iron ore. (a) Massive hematite vein within the dolomitic limestone (b) Massive hematite. (c) Cavity-filling botryoidal goethite on a dolomitic limestone. (d) Hematite formed as oxidation of sulphide minerals. (e) Limonite pseudomorph after hematite. (f) Fe-oxides on rosettes of barite crystals

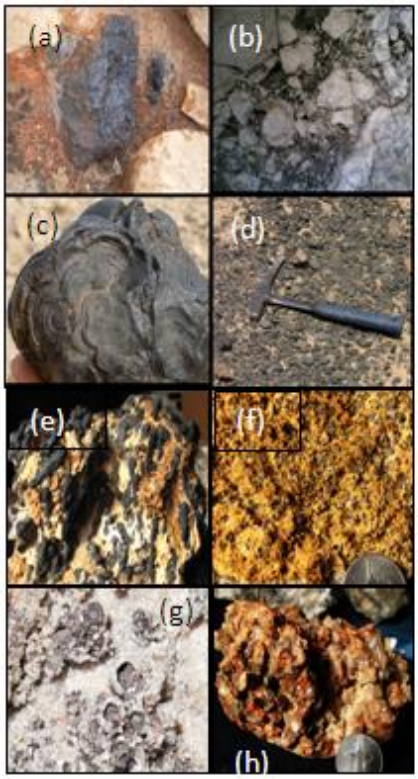

Fig. 6. Different structures and textures of manganese ore. (a) Cryptomelane massive vein. (b) Stockwork brecciated limestone cemented by manganese ore. (c) Botryoidal texture (d) Hollandite and romanechite fragments associated with carbonate sediments. (e) Cryptomelane impregnatively penetrating carbonate rock. (f) Dissemination and patches of manganese ore in the calcareous rock. (g) Spheroids of manganese oxides and hydroxides. (h) Rodochrosite with calcite crystals

4.1.2 Manganese ores

Manganese ores occur as small massive veins (Fig. 6a) several meters long, ranging in width from centimetres to 1m; as stockwork mineralization cementing brecciated carbonate rocks (Fig. 6b); and as cavity and pore filling characterized by botryoidal structure (Fig.6c). Hollandite and pyrolusite fragments up to 20 cm in diameter are scattered and particularly associated with the debris carbonate sediments (Fig. 6d). Manganese ores also impregnatively penetrate the host rocks to a considerable depth (Fig. 6e). The Mn mineralization often occurs as disseminations and patches (Fig. 6f) in the calcareous rocks (Fig.6g). Rodochrosite occurs in association with calcite in the northwestern part of Al-Kohl1 prospect (Fig.6h). Hollandite, romanechite, and cryptomelane form thin acicular crystals with spherulitic texture. Their colour is dark grey, or black. In Table 2, the relative proportions of hollandite and romanechite in two differently mineralised samples are reported. Pyrolusite occurs either in small massive veins or as small pieces ranging up to 20cm in diameter.

Table 2. Quantitative XRD results of two manganese ore samples from WMB

Mineral	MAM-432 (wt.%)	MAM-436 (wt.%)
Hollandite	100	27
Romanechite	-	45
Quartz	-	18
Anhydrite	-	9
Total	**100**	**99**

4.2 Geochemistry of Fe-Mn ores

Whole rock chemical analyses for major and trace elements of Fe-Mn orebodies, Fe-Mn disseminated carbonate rocks, and non-mineralised carbonates, are summarised in Table 3.

Iron orebodies are mainly high-grade, with the highest iron contents (~80-74% Fe_2O_3) associated to massive hematite. The mineralised veins have variable tenors of Fe_2O_3, from ~ 52% down to ~11%. Cr and Zn contents can be up to 6,000 and 5,000 ppm, respectively, in some low-grade specimens. Samples characterized by high Pb contents (~1-2% Pb) have low tenors in Fe_2O_3. The manganese orebodies have mostly high Mn tenors (~65-52% MnO). All of them are characterised by high Pb (up to 4.4%), Ba (up to >1%), and Zn (up to ~4,800 ppm) contents. The mineralised vein MAM-2032, with a content of 49.50% MnO, is highly enriched in Zn (23%), Pb (1.6%), and Cd (>1%).

Fe/Mn ratios vary from about 30,000 (74% Fe_2O_3) for a massive hematite body to about 0.004 (65% MnO) for a massive pyrolusite lens.

Fe and Mn minerals are sometimes finely dispersed throughout the carbonate rocks to the extent that it may be difficult distinguishing mineralised from non-mineralised rocks. For the purposes of the present study, a divide was arbitrarily set at 4% Fe_2O_3 and 0.6% MnO, based on the maximum known concentrations in non-mineralised carbonates [e.g. 19,19]. The disseminated ores hereby delimited, are considerably lower-grade with respect to the Fe and Mn orebodies; they display, however, significant tenors of Fe_2O_3 (up to ~13%) and MnO (up to ~5%). Their Pb and Zn contents can locally be very high (over 1% and up to ~0.5%, respectively).

Variations in contents of selected major elements with depth for the drillcore samples are shown in the plot of Fig. 7. The rocks drilled are mostly limestones that, near the surface, are dolomitised. They have variable contents of Fe and Mn, both of which are higher topside, and, with the exception of Fe in borehole BH1, tend to decrease with increasing depth. All drillcore samples are, however, low-grade in both Fe (~4-0.3%) and Mn (~0.6-0.1%).

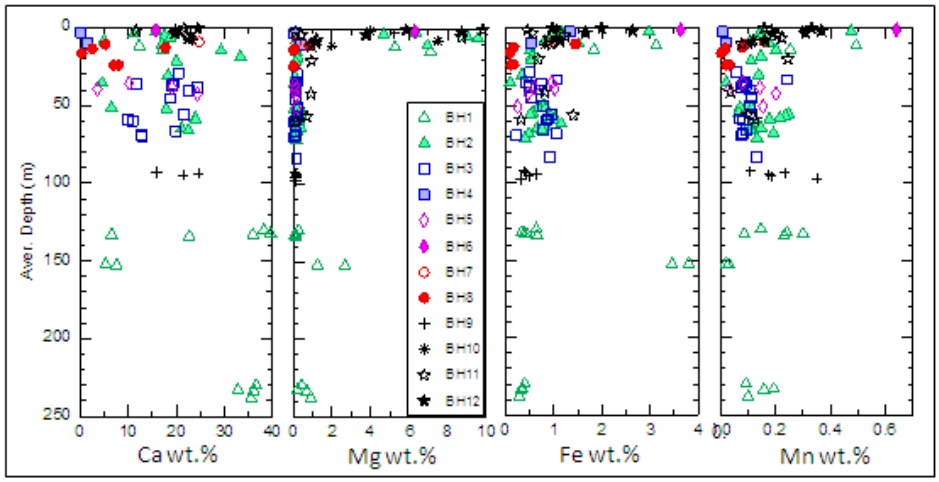

Fig. 7. Variation of Ca, Mg, Fe, and Mn (wt.%) with depth (m) in the 12 drillcores from Alkohl1

Table 3. Results of whole rock chemical analyses for major (wt.%) and trace elements (ppm) of mineralised rocks, and non-mineralised carbonates, from WMB

SAMPLE	Description	Location		AM(*)	Fe2O3	MnO	CaO	MgO	Al2O3	K2O
					wt %	wt %	wt %	wt %	wt %	wt %
Iron orebodies		LON East	LAT North							
MAM-437	Small blocks of hematite	499266	1705713	1	79.79	0.12	0.69	0.13	0.45	0.01
MAM-85	Hematite block	510146	152322	2	73.86	0.00	0.55	0.27	0.47	0.10
MAM-2128	Vein of dark brown hematite	498796	1702635	3	52.34	0.03	0.94	0.03	0.26	0.02
MAM-2088	Vein of hematite	501271	1700710	3	45.62	0.09	8.59	0.22	0.51	0.02
MAM-2177	Brownish black hematite block	-	-	1	44.04	0.02	1.41	0.30	0.49	0.04
MAM-2169	Hematite vein	500229	1704925	1	38.61	0.34	0.74	0.12	0.26	0.01
MAM-2180	Oxidised hematite vein	501039	1702038	1	35.61	0.48	0.83	0.17	0.32	0.01
MAM-2158A	Hematite veinlets+barite	500223	1705179	1	31.60	0.04	3.06	0.10	0.11	<0.01
MAM-2179	Hematite with barite+oxidized galena	501039	1702038	1	25.74	0.08	0.29	0.05	0.04	<0.01
MAM-435	Dark brown to yellowish hematite+limonite	501039	1702038	1	22.02	0.09	3.02	0.07	0.09	0.01
MAM-2122	Vein of hematite+barite+limonite	506219	1700213	3	17.23	0.06	4.29	0.38	0.76	0.05
MAM-2133	Dike of hematite+limonite+galena	498523	1702584	3	12.87	0.04	2.03	0.08	0.43	0.04
MAM-2	Mineralised vein	510146	152322	2	14.07	2.33	2.27	0.75	1.23	0.29
MAM-2075	Silicified vein of quartz+hematite	499949	1701962	3	16.45	0.03	3.68	0.35	0.66	0.13
MAM-2078	Brownish-reddish hematite vein	499552	1702082	3	10.31	0.02	1.44	0.23	0.66	0.07
MAM-2107	Yellowish compact limonitised hematite	503558	1698164	3	10.11	0.05	2.92	0.18	1.40	0.17
MAM-2131	Silicified grey to dark grey limestone	498177	1702807	3	11.37	0.04	2.11	0.05	0.36	0.02
Manganese orebodies										
C.1	Massive pyrolusite lens	-	-	2	<0.01	61.61	1.62	0.66	<0.02	0.22
C.2	Massive pyrolusite lens	-	-	2	0.06	61.37	1.85	0.99	0.13	0.25
MAM-92	Manganese ore	498641	1706735	2	0.31	61.37	3.04	0.10	1.15	0.17
MAM-432	Lenses of manganese ore	498612	1706717	1	0.26	64.83	1.30	0.25	1.51	0.23
MAM-433	Lenses of manganese ore	498543	1706595	1	0.13	51.92	2.62	<0.02	1.02	0.17
MAM-2032	Mineralised vein	499223	1701380	3	1.63	49.50	17.42	0.48	0.49	0.08

SAMPLE	Description	Location		AM(*)	Fe2O3	MnO	CaO	MgO	Al2O3	K2O
					wt %	wt %	wt %	wt %	wt %	wt %
MAM-436	Lens of manganese ore, needle-like crystals	498951	1705605	1	0.23	47.60	2.38	0.02	0.79	0.16
MAM-2061	Mineralised vein	498711	1701955	3	1.54	8.70	14.34	0.23	0.45	0.06
Fe-Mn disseminated carbonate rocks										
MAM-0	Yellowish limestone	510146	152322	2	2.37	0.67	52.88	1.03	0.96	0.33
MAM-8	Yellow limestone	510146	152322	2	7.66	0.31	29.66	0.80	1.25	0.34
MAM-89	Yellowish to brownish altered limestone	498897	1706849	2	0.69	3.11	30.08	18.74	0.62	0.20
MAM-93	Grey limestone	498957	1706809	2	1.50	3.98	34.70	12.83	0.72	0.29
MAM-133	Red-rose dolomitic limestone	494480	1706225	2	4.95	0.30	39.45	8.49	0.77	0.30
MAM-429	Silicified limestone	498560	1706713	1	0.57	1.27	24.48	0.93	0.15	0.10
MAM-441	Dark limestone	501700	1701800	1	3.93	4.87	39.87	0.41	0.17	0.01
MAM-2020	Silicified limestone	501682	1701933	1	0.70	0.69	28.54	0.36	0.36	0.10
MAM-2067	Brecciated limestone vein	498924	1701248	3	8.91	0.01	43.09	3.43	0.43	0.13
MAM-2069	Calcite vein	499291	1701300	3	12.53	1.33	45.05	0.60	0.60	0.07
MAM-2080	Calcite vein	499398	1702151	3	4.53	0.41	49.66	0.15	0.42	0.11
MAM-2126	Compact/ porous reddish limestone	499135	1701663	3	12.91	0.13	41.41	0.38	0.68	0.01
MAM-2127	Silicified pale brown to yellowish limestone	498793	1702682	3	11.24	0.09	39.45	0.08	0.94	0.20
MAM-2158B	Pyrolusite-rich aragonite veinlets	500224	1705180	1	1.34	2.06	39.87	0.32	0.09	0.02
Non-mineralised carbonate rocks										
MAM-124	Grey limestone	502397	1701494	2	0.92	0.75	33.58	0.35	1.00	0.33
MAM-125	Silicified limestone	502531	1701243	2	1.56	0.12	21.40	1.82	0.40	0.12
MAM-427	Silicified limestone	498554	1706750	3	0.33	0.11	25.18	0.17	0.02	<0.01
MAM-2049	Grey compact limestone	500170	1701414	3	0.40	0.01	40.01	1.09	0.25	0.05
MAM-2050	Fine-grained red-rose dolostone	500250	1701450	3	0.03	0.00	49.24	16.83	0.04	<0.01
MAM-2051	Silicified fossiliferous limestone	499606	1701415	3	1.46	0.08	33.58	2.16	0.19	0.05
MAM-2055	Silicified limestone	500030	1701480	3	1.13	0.08	41.13	0.96	0.23	0.06
MAM-2057	Yellowish to brownish altered limestone	499300	1701839	3	1.62	0.19	50.22	0.15	0.45	0.12
MAM-2068	Reddish, yellow to brownish limestone	499027	1701301	3	0.83	0.08	51.06	0.65	0.83	0.31

SAMPLE	Description	Location		AM(*)	Fe2O3	MnO	CaO	MgO	Al2O3	K2O
					wt %	wt %	wt %	wt %	wt %	wt %
MAM-2070	Yellowish compact limestone	499446	1701138	3	0.94	0.13	39.87	0.85	0.60	0.12
MAM-2073	Silicified limestone	499880	1701658	3	0.79	0.15	52.88	0.83	0.45	0.17
MAM-2074	Silicified limestone	500088	1701749	3	1.13	0.03	50.08	0.18	0.81	0.18
MAM-2076	Grey limestone	499696	1702001	3	0.99	0.20	47.57	0.43	0.98	0.36
MAM-2096	Grey limestone	503192	1698905	3	0.46	0.16	49.38	0.17	0.13	0.02
MAM-2097	Yellowish compact silicified limestone	503199	1698927	3	0.39	0.21	51.06	0.07	0.19	0.05
MAM-2111	Slightly silicified yellowish limestone	501519	1700661	3	0.77	0.63	51.06	0.96	0.11	0.04
MAM-2138	Silicified limestone	499968	1701660	3	1.32	0.08	27.84	0.08	1.23	0.40
MAM-2146	Yellow limestone	499834	1701501	3	1.73	0.02	44.49	0.03	1.17	0.37

(*) Analytical Methods: 1=ME-ICP41+OG46; 2=ME-MS61+OG62; 3=ME-ICP61+OG62. - = not analysed

Table 3. Continued

SAMPLE	Na2O	TiO2	SO3	Ag	As	Ba	Be	Cd	Ce	Co	Cr	Cu
	wt %	wt %	wt %	ppm	ppm	ppm	ppm	ppm	ppm	ppm	ppm	ppm
Iron orebodies												
MAM-437	0.04	0.08	0.85	1.7	12	420	<0.5	<0.5	-	<1	881	3
MAM-85	0.11	0.03	0.72	0.6	228	4610	2.3	1.1	3.3	31	30	32
MAM-2128	0.03	0.12	0.70	2.3	33	1390	0.8	<0.5	-	<1	15	11
MAM-2088	0.04	0.05	0.97	1.1	113	490	8.3	1.2	-	<1	1905	67
MAM-2177	0.11	0.02	0.47	0.5	22	760	<0.5	<0.5	-	17	3	42
MAM-2169	0.05	<0.02	0.62	0.8	76	730	11.5	<0.5	-	<1	33	14
MAM-2180	0.05	<0.02	0.82	0.5	79	430	13.5	4.5	-	<1	41	12
MAM-2158A	0.07	0.02	0.45	0.2	61	1220	2.2	1.6	-	1	16	7
MAM-2179	0.01	<0.02	0.37	<0.2	62	660	0.8	1.2	-	1	19	13
MAM-435	0.03	0.23	0.32	<0.5	20	360	0.5	1.0	-	<1	2760	13
MAM-2122	0.03	0.12	0.92	0.7	118	1910	2.4	<0.5	-	8	16	21
MAM-2133	0.04	0.12	0.77	9.8	100	2300	2.1	0.8	-	7	28	107
MAM-2	0.08	0.07	0.55	0.7	142	1100	25.5	0.6	9.0	24	22	10
MAM-2075	1.42	0.10	3.02	3.2	77	490	1.3	16.2	-	6	6210	58
MAM-2078	0.03	0.13	0.62	3.3	114	660	0.5	4.5	-	5	3410	95

SAMPLE	Na2O	TiO2	SO3	Ag	As	Ba	Be	Cd	Ce	Co	Cr	Cu
	wt %	wt %	wt %	ppm	ppm	ppm	ppm	ppm	ppm	ppm	ppm	ppm
MAM-2107	0.07	0.25	1.65	1.1	30	1290	1.1	<0.5	-	14	34	10
MAM-2131	0.03	0.02	1.02	6.4	161	2080	0.5	1.1	-	5	7	88
Manganese orebodies												
C.1	0.40	0.01	0.85									
C.2	0.44	0.02	0.62									
MAM-92	0.03	0.03	0.12	0.1	25.3	>1%	8.4	1.4	41.5	900	15	419
MAM-432	2.45	0.05	<0.02	5.2	36	>1%	11.1	0.6	-	1210	<1	723
MAM-433	2.47	0.02	0.15	10.5	33	>1%	10.9	4.0	-	1160	1000	648
MAM-2032	0.04	0.05	0.72	7.6	<5	700	1.0	>1%	-	142	6	235
MAM-436	1.25	0.02	<0.02	3.9	52	>1%	15.1	2.9	-	1000	199	358
MAM-2061	0.07	0.02	0.17	0.8	45	3530	5.5	1.7	-	152	169	74
Fe-Mn disseminated carbonate rocks												
MAM-0	0.04	0.08	0.30	0.2	23	830	0.8	0.7	28.0	5	5	13
MAM-8	0.12	0.07	1.05	0.6	56	1640	3.9	20	11.8	6	8	21
MAM-89	0.03	0.05	0.12	0.0	12	6090	1.3	2.1	14.5	60	3	29
MAM-93	0.01	0.04	0.40	0.1	8	8190	1.4	7.1	19.4	69	4	32
MAM-133	0.03	0.05	0.50	0.0	27	400	2.0	2.1	11.9	7	4	25
MAM-429	<0.01	<0.02	10.74	0.3	6	80	<0.5	9.7	-	2	9	6
MAM-441	0.11	<0.02	<0.02	0.9	88	6100	3.0	36	-	68	28	136
MAM-2020	0.03	<0.02	<0.02	<0.2	<2	1280	<0.5	<0.5	-	1	7	38
MAM-2067	0.01	0.02	0.87	<0.5	80	160	2.9	2.7	-	<1	23	23
MAM-2069	0.03	0.02	0.82	<0.5	128	1760	11.9	2.6	-	94	8	24
MAM-2080	0.01	0.03	0.07	<0.5	28	170	0.5	<0.5	-	2	10	3
MAM-2126	<0.01	0.02	0.67	<0.5	318	3280	11.4	15	-	5	5	62
MAM-2127	0.04	0.07	0.12	0.5	15	370	1.5	1.3	-	2	10	12
MAM-2158B	0.19	<0.02	0.35	0.4	52	3550	3.4	9.2	-	22	1	13
Non-mineralised carbonate rocks												
MAM-124	0.04	0.06	0.52	0.9	<5	1420	1.4	29	54.9	4	5	11
MAM-125	0.01	0.03	0.57	0.3	23	1200	0.4	2.1	6.7	2	22	24
MAM-427	0.03	<0.02	<0.02	0.2	2	2250	<0.5	2.0	-	1	273	4
MAM-2049	<0.01	0.02	0.35	<0.5	6	1460	<0.5	4.8	-	3	229	14
MAM-2050	0.03	<0.02	0.57	<0.5	<5	200	<0.5	17	-	<1	8	2

SAMPLE	Na2O	TiO2	SO3	Ag	As	Ba	Be	Cd	Ce	Co	Cr	Cu
	wt %	wt %	wt %	ppm	ppm	ppm	ppm	ppm	ppm	ppm	ppm	ppm
MAM-2051	0.04	0.02	1.57	<0.5	11	300	<0.5	63	-	2	13	3
MAM-2055	0.01	0.02	1.07	<0.5	8	160	<0.5	2.5	-	1	24	<1
MAM-2057	0.01	0.05	0.07	<0.5	26	120	0.5	1.0	-	2	22	4
MAM-2068	0.03	0.07	0.50									
MAM-2070	0.09	0.05	0.40	<0.5	23	120	0.7	24	-	12	22	6
MAM-2073	0.05	0.03	0.15	<0.5	16	120	<0.5	26	-	1	24	1
MAM-2074	0.13	0.05	0.57	<0.5	29	4300	0.9	56	-	6	44	7
MAM-2076	0.04	0.08	0.30	<0.5	25	3050	0.9	50	-	3	142	11
MAM-2096	0.01	0.02	0.02	<0.5	<5	110	<0.5	<0.5	-	1	12	3
MAM-2097	<0.01	0.02	0.05	<0.5	8	540	<0.5	<0.5	-	3	15	4
MAM-2111	<0.01	<0.02	0.10	<0.5	<5	390	<0.5	0.9	-	1	2	4
MAM-2138	0.03	0.10	0.47	<0.5	21	1120	0.7	96	-	5	8	13
MAM-2146	0.03	0.07	0.15	<0.5	30	660	1.3	78	-	1	13	5

Table 3. Continued

SAMPLE	La	Mo	Nb	Ni	P	Pb	Rb	Sr	V	Y	Zn	Zr
	ppm	ppm	ppm	ppm	ppm	ppm	ppm	ppm	ppm	ppm	ppm	ppm
Iron orebodies												
MAM-437	<10	35	-	62	240	-	-	169	249	-	967	-
MAM-85	2	174	0.9	529	480	721	4	264	329	3.3	5110	6
MAM-2128	<10	22	-	8	310	227	-	1010	104	-	114	-
MAM-2088	<10	20	-	142	870	1220	-	1870	460	-	2140	-
MAM-2177	<10	41	-	40	120	113	-	276	16	-	240	-
MAM-2169	<10	10	-	23	470	81	-	175	752	-	1155	-
MAM-2180	10	13	-	25	410	100	-	230	962	-	2680	-
MAM-2158A	<10	8	-	4	710	139	-	319	172	-	1305	-
MAM-2179	<10	8	-	4	50	1170	-	2110	149	-	1280	-
MAM-435	<10	5	-	211	100	>1%	-	82	226	-	297	-
MAM-2122	<10	4	-	26	490	147	-	254	169	-	786	-
MAM-2133	10	19	-	16	90	1.37%	-	264	60	-	1215	-
MAM-2	4	85	6.9	23.7	250	1.77%	10	2980	41	2.9	2970	36
MAM-2075	<10	19	-	431	170	389	-	294	60	-	2700	-

SAMPLE	La	Mo	Nb	Ni	P	Pb	Rb	Sr	V	Y	Zn	Zr
	ppm	ppm	ppm	ppm	ppm	ppm	ppm	ppm	ppm	ppm	ppm	ppm
MAM-2078	10	8	-	247	200	4760	-	2210	17	-	790	-
MAM-2107	10	3	-	31	400	98	-	303	65	-	706	-
MAM-2131	<10	5	-	11	110	1600	-	171	8	-	811	-
Manganese orebodies												
MAM-92	40	348	2.2	114	180	2.34%	4	6150	1910	8.5	3090	13
MAM-432	40	424	-	191	300	4.37%	-	5500	2440	-	4270	-
MAM-433	20	398	-	172	880	0.90%	-	6280	2100	-	4350	-
MAM-2032	<10	85	-	8	120	1.64%	-	1720	1815	-	2360	-
MAM-436	50	471	-	104	100	1.22%	-	>1%	1310	-	4790	-
MAM-2061	<10	151	-	40	80	1.06%	-	8540	75	-	1280	-
Fe-Mn disseminated carbonate rocks												
MAM-0	13	6	3.6	2.1	80	236	13	467	13	7.3	83	21
MAM-8	7	13	6.8	26.2	280	3950	12	222	61	4	2650	48
MAM-89	7	25	2.3	9.6	40	1180	7	647	123	3.1	458	14
MAM-93	8	33	3.1	16	120	1700	7	952	155	4.7	1355	21
MAM-133	6	11	4.2	15.6	120	1150	10	432	77	4.1	1090	27
MAM-429	<10	12	-	3	140	891	-	931	25	-	563	-
MAM-441	<10	35	-	76	320	1.04%	-	923	228	-	4630	-
MAM-2020	<10	3	-	3	100	68	-	816	7	-	361	-
MAM-2067	<10	19	-	29	70	3720	-	702	17	-	4330	-
MAM-2069	<10	51	-	46	180	3370	-	835	71	-	5230	-
MAM-2080	<10	4	-	13	30	45	-	245	28	-	255	-
MAM-2126	<10	5	-	15	160	2370	-	296	221	-	1820	-
MAM-2127	<10	6	-	13	520	91	-	211	147	-	654	-
MAM-2158B	<10	14	-	66	50	542	-	1160	120	-	831	-
Non-mineralised carbonate rocks												
MAM-124	24	7	6.5	4	120	4870	12	1605	17	10.3	741	43
MAM-125	3	14	2.2	7.6	120	4320	4	2250	90	2.3	1430	14
MAM-427	<10	6	-	43	30	699	-	171	125	-	183	-
MAM-2049	<10	<1	-	21	80	2130	-	2010	232	-	1610	-
MAM-2050	<10	<1	-	3	100	1070	-	1020	10	-	8470	-
MAM-2051	<10	2	-	5	40	214	-	642	9	-	2490	-

SAMPLE	La	Mo	Nb	Ni	P	Pb	Rb	Sr	V	Y	Zn	Zr
	ppm	ppm	ppm	ppm	ppm	ppm	ppm	ppm	ppm	ppm	ppm	ppm
MAM-2055	10	1	-	4	40	177	-	283	11	-	583	-
MAM-2057	<10	2	-	11	50	71	-	189	5	-	52	-
MAM-2068												
MAM-2070	<10	2	-	6	100	835	-	4910	13	-	2360	-
MAM-2073	<10	2	-	6	100	449	-	422	9	-	1360	-
MAM-2074	<10	2	-	26	210	1135	-	430	19	-	7490	-
MAM-2076	<10	1	-	15	170	745	-	296	14	-	791	-
MAM-2096	<10	<1	-	16	20	3	-	224	7	-	28	-
MAM-2097	<10	1	-	10	40	6	-	275	7	-	19	-
MAM-2111	<10	3	-	4	40	4	-	405	7	-	107	-
MAM-2138	<10	<1	-	18	120	364	-	3790	17	-	5660	-
MAM-2146	<10	9	-	8	130	3400	-	245	59	-	2070	-

5. DISCUSSION

Given the oxidation and upgrading of the ore deposit (see § 4.1), which suggest intense circulation of meteoric waters in a relatively young fracture system, evaluating the compositional changes that accompany post-depositional patterns formed in the secondary environment is advisable. With this in mind, the mobile versus immobile behaviour of some elements should, if possible, be distinguished. In this regard, vanadium is used here as a control element of primary element distribution in the deposit. Carbonate rocks have quite low V contents: [21] reported values <15 ppm for pure carbonate sediments; data for limestones from various depositional environments, including the coastal area of Yemen near Al-Mukalla, amount to < 40 ppm [22,23,24]. Although [25] observed that V might be enriched in marine sediments under oxygen-depleted conditions, Enrichment Factors (EF) reported in the paper reach 0.8 at most, whereas the carbonate rocks from WMB have vanadium EF up to 33. Hence, we are confident that high V contents in WMB rocks mostly reflects the abundance of Fe and Mn minerals. Accordingly, the positive correlation between V and Mn in most WMB rocks suggests that Mn and V are paragenetically associated, which, in turn, could be interpreted as a common origin. On this basis, since Rb, Sr, Ba, and Pb fluctuations are not correlated with those of V, these elements were likely mobilised during secondary alteration. Conversely, the positive correlation of La, Co, Cu, Ni, and Zn with V suggests that these elements remained quite immobile during secondary processes and therefore they can be used to infer on the origin of the mineralising fluids.

Iron-manganese deposits occur in nearly all tectonic environments. Generally speaking, they may be formed by one or more of four processes [26,27,28]: (1) precipitation from hydrothermal fluids, (2) hydrogenetic precipitation from either marine or ambient water, (3) precipitation from sediment pore waters that have been modified from bottom water compositions by diagenetic reactions in the sediment column and (4) replacement of rocks and sediments. Different sources of the mineralising fluids influence the geochemical features of the deposits, such as the Fe/Mn ratio [29]. In addition, significant indicators used to identify different genetic types of mineralisation are the contents of transition metals such as Cu, Co, Ni, and Zn [28,30].

In the discrimination diagram proposed by [28], in Fig.8a, the WMB Fe-Mn ores plot in the field of hydrothermal conditions of formation.

In the ternary discrimination diagram of Fig. 8b (after [30]), the WMB Fe orebodies plot, as expected, on the Fe corner and the Mn ones plot on the Mn corner. The Fe-Mn disseminations, instead, have variable Mn/Fe ratios that spread all over the Fe-Mn axis. They show quite low (Cu+Ni+Co) for most Mn/Fe. Such a distribution seems to fit fairly well the field representing ferromanganese deposits of hydrothermal origin. It should be noted, however, that the fields of hydrothermal and diagenetic deposits overlap at the Mn corner. It could not therefore be excluded a contribution from a diagenetic process as well.

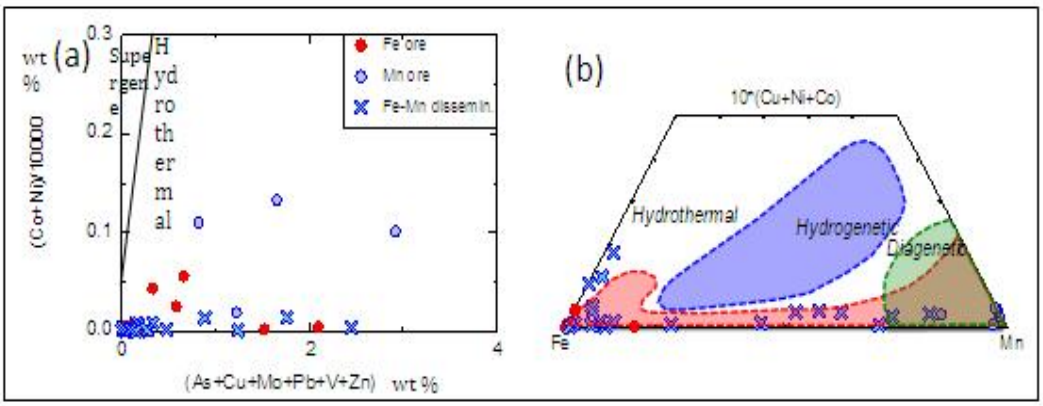

Fig. 8. Plot of WMB Fe-Mn ore composition on: (a) trace element discrimination binary diagram for deposits of supergene and hydrothermal origin after [28]); (b) ternary discrimination system of Fe-Mn deposits after [30]

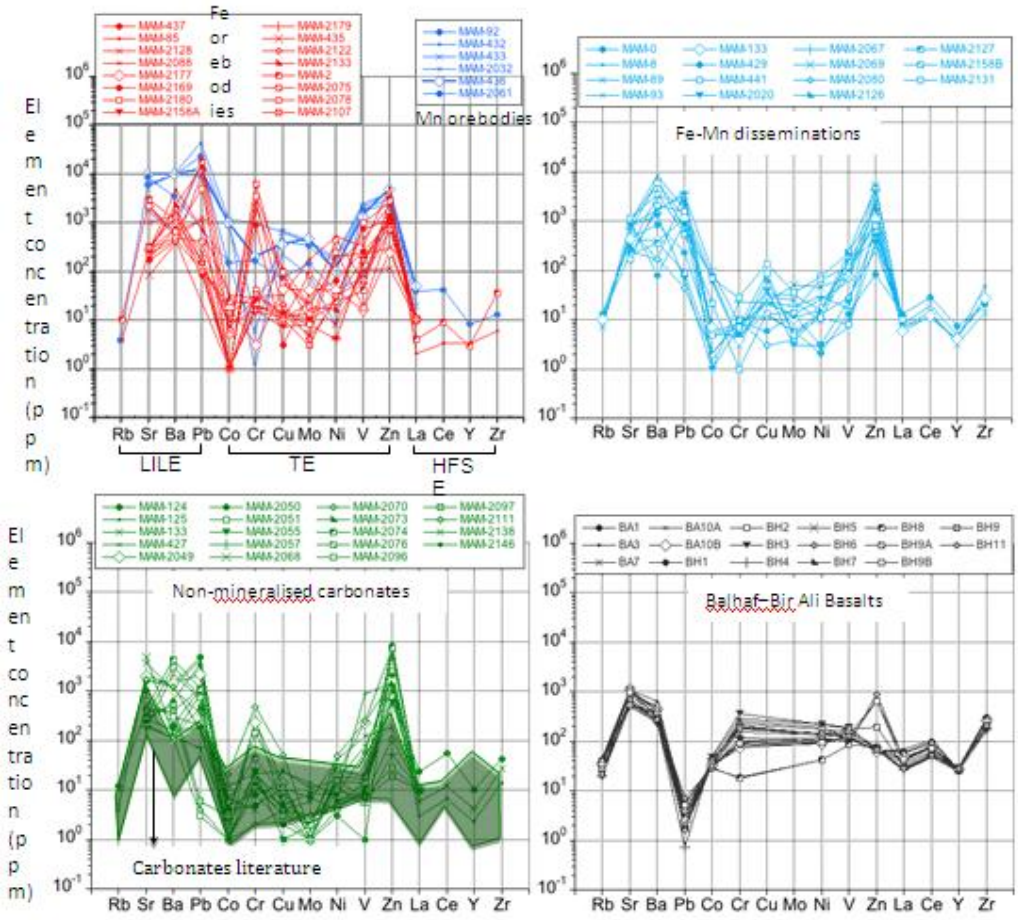

Fig. 9. Spidergrams showing the trace element concentrations (ppm) in WMB rocks. (a) Fe and Mn orebodies. (b) Fe-Mn disseminations in carbonate rocks. (c) Non-mineralised carbonates. The field representative of carbonates from literature is after [31,23,24,32]. (d) Quaternary basalts from the Balhaf–Bir Ali volcanic field [18], which crops out near to WMB, taken as representatives of the local magmatic system

Mineralising hydrothermal fluids could be derived from the magmatic-hydrothermal system connected to the Quaternary volcanic rocks occurring in the southeastern part of WMB (see sections 2.1 and 2.2). This hypothesis can be evaluated by comparing the chemistry of the ores to the one of the outcropping igneous rocks (Fig. 9). For this purpose, the basalts from the Balhaf–Bir Ali volcanic field [18], which crops out near to the WMB, were taken as representatives of the local magmatic system. In addition, a possible contribution from diagenetic water and/or near surface waters could be elucidated by comparison with the chemistry of the carbonate country rocks (Fig. 9).

Observing the trace element patterns of Fig. 9, the following remarks can be made:

(i) Overall, high Ba, Pb, Cr, and Zn concentrations in all the WMB rocks are consistent with barite-polymetallic mineralisation associated to the Fe-Mn ore (see § Geology of Wadi Masilah Basin). These elements have variations in the absolute contents up to four orders of magnitude, and sometimes produce crosscutting patterns with positive versus negative spikes. This is likely due to the mechanism of fluid transport that may cause dissolution or re-precipitation of some elements depending on the local redox conditions.

(ii) The Fe ores (Fig. 9 a, red colour) have very low concentrations of Rb and Co whereas the other Large Ion Lithophile Elements (LILE) are distinctly enriched, thus describing a characteristic bell-shaped pattern. Among the Transition Elements (TE), Cr an Zn display positive spikes of variable extents, whereas High Field Strength Elements (HFSE) have much lower contents, with a smaller positive spike of Ce.

(iii) The Mn ores (Fig. 9 a, blue colour) have trace element patterns similar in shape to those of the Fe ores, but differ for the higher absolute concentrations of most elements, and for a mainly negative spike of Cr.

(iv) The Fe-Mn disseminations, (Fig. 9 b) have trace element patterns similar to those of Mn ores, but a positive spike of Cu in some samples.

(v) The non-mineralised WMB carbonates (Fig. 9 c) have trace element patterns surprisingly similar to those of Fe ores, with some samples enriched in LILE, Cr, and Zn with respect to widespread carbonate rocks. This is likely due to a dissemination of mineralised minerals in such a fine dispersion that it may be difficult to fully remove them from the host carbonate rocks.

(vi) The patterns of Quaternary basalts (Fig. 9 d) differ from those of Fe-Mn ores for having lower LILE contents, particularly Pb that exhibit a deep negative spike, and higher Ni contents. In the right part of the plot, instead, from Zn to HFSE, the basalts have patterns similar in shape to those of the mineralisation, with positive spikes of Zn in some samples, to a lesser extent, low HFSE, and positive Ce spike. This suggests that basalts could represent a possible source of Zn and HFSE, whereas for LILE and Pb a supplemental source should be envisaged.

The overall Ce positive spike of the WMB rocks may provide further evidence about the mineralising fluids. In oxidizing environments the soluble Ce^{3+} is oxidized into insoluble Ce^{4+} that tend to precipitate as CeO_2 along with Mn and/or Fe oxyhydroxides [33,34]. The Ce positive spike of the WMB rocks thus suggests a shallow, oxidizing environment of deposition. Consequently, shallow level fluids originating from the local drainage system, could have supplied additional LILE and Pb.

6. CONCLUSION

Fe-Mn mineralisation of WMB may be (i) structurally controlled, (ii) randomly oriented depending on the occurrence of brittle structures, cavities and vugs, (iii) or finely disseminated in the carbonate host rocks. The mineralogical assemblage consists of hematite, limonite, and goethite in the Fe orebodies; hollandite, romanechite, cryptomelane, pyrolusite, and rodochrosite in the Mn orebodies.

Both iron and manganese ores are mainly high-grade. Fe_2O_3 contents are ~80-74% in massive hematite orebodies, and range from ~ 52% to ~11% in the mineralised veins. MnO contents are ~65 to 52% in massive pyrolusite orebodies, and range from ~ 52% to ~9% in the mineralised veins. The disseminated Fe-Mn ores are considerably lower-grade, but display however significant tenors of Fe_2O_3 (up to ~13%) and MnO (up to ~5%). Drillcore samples are mostly limestones and dolomitic limestones variably enriched in Fe and Mn, whose tenors are higher near the surface, and tend to decrease with increasing depth. They are low-grade in both Fe_2O_3 (~6-0.4%) and MnO (~0.8-0.1%).

Geochemical signatures of major and trace elements provided evidence about the source of the mineralising fluids. Discriminative diagrams based on Fe/Mn and transition metals support a hydrothermal origin with possible contribution from diagenetic processes. The distribution of Zn and HFSE suggests that hydrothermal mineralising fluids are related to the magmatic-hydrothermal systems affiliated to the neighbouring Quaternary volcanic fields. Widespread positive Ce spikes in the trace element patterns suggest the Fe-Mn mineralisation took place in a relatively shallow, oxidizing environment.

ACKNOWLEDGEMENTS

This work was financially supported by MEMC Inc. and Naine Minerals and Energy and Mining (AJHAM) Companies, and by the Geological Survey and Minerals Resources of Yemen.

COMPETING INTERESTS

Authors have declared that no competing interests exist.

REFERENCES

1. Nehlig P, Salpeteur I, Asfirane F, et al. The Mineral Potential of the Arabian Shield: A reassessment. IUGS/UNESCO Deposits Modeling Workshop. USGS - Spec Pub; 1999.
   DOI: 10.13140/RG.2.1.1889.9282:51.
2. Abdulameer WA. The Mineral Industry of Yemen. In: Minerals Yearbook - Yemen. US Geological Survey. 2014;66:1-66.7.
3. Pinarelli L, Mattash MA. Mineral Resources in the Red Sea/Gulf of Aden: Polymetallic-Barite Mineralizations at Wadi Masilah Basin (Yemen). In: Robbins D, editor. Red Sea: Historical Significance, Properties and Economic Importance. Series: Earth Sciences at the 21th Century, Nova Science Publishers. 2018;47-76.
4. Mattash MA, Al-Ameri AA, Shaqra AA. Geology and geochemistry of barite prospect in Yemen. In: Sixth International Symposium on Eastern Mediterranean Geology incorporating the Ninth International Conference of Jordanian Geologists Association. 2007;249-250.
5. Mattash MA, Shaqra AA, Al-Ameri AA. Geological survey and feasibility study of pyrolusite deposit in Yemen. In: Sixth International Symposium on Eastern Mediterranean Geology incorporating the Ninth International Conference of Jordanian Geologists Association. 2007:251-252.
6. Mattash MA. Geology and geochemistry of the sedimentary-hosted lead-zinc-vanadium-barite prospects in Yemen. In: International Geological Congress, Oslo-Norway; 2008.
7. Mattash MA, Al-Ameri AA, Shaqra AA Geology and geochemistry of the carbonate hosted polymetallic-barite prospects in Wadi Al-Masila, Al-Mahrah province, Yemen. In: Second Syrian Geological Conference, Damascus, Syria; 2009.
8. Haitham FM, Nani ASO. The Gulf of Aden rift: hydrocarbon potential of the Arabian sector. J Pet Geol. 1990;13:211–220.
9. Bott WF, Smith BA, Oakes G, Sikander AH, Ibrahim AI. The tectonic framework and regional hydrocarbon prospectivity of the Gulf of Aden. J Pet Geol. 1992;15:211–243.
10. Redfern P, Jones JA. The interior rifts of the Yemen - analysis of basin structure and stratigraphy in a regional plate tectonic context. Basin Res. 1995;7:337-356.
11. Ellis AC, Kerr HM, Cornwell CP, Williams DO. A tectonostratigraphic framework for Yemen and its implications for hydrocarbon potential. Petrol Geosci: 1996;2:29-42.
12. Beydoun ZR, As-Saruri M, Baraba RS. Sedimentary basins of the Republic of Yemen: their structural evolution and geological characteristics. Rev Inst Franc Petrol. 1996;51:763-775.
13. Al-Areeq NA, Elhossainy ME, Salman AM. Sequence stratigraphic architecture of the Upper Jurassic-Lower Cretaceous deposits in the Sayun-Masilah Basin, Yemen: A case study from Masilah oilfields. J Asian Earth Sci. 2020;191.
    Article 104287.
14. As-Saruri M, Sorkhabi R. Petroleum basins of Yemen. Geo Ex Pro. 2016;13(2):38-42.
15. Mattash MA, Pinarelli L, Vaselli O, et al. Geochemical evolution of southern Red Sea and Yemen flood volcanism: evidence for mantle heterogeneity. Arab J Geosci. 2014;7(11):4831-4850.
16. Mallick DIS, Gass IG, Cox KG, De vries BVW, Tindle AG Perim Island, a volcanic remnant in the southern entrance to the Red Sea. Geol Mag. 1990;127:309–318.
17. As-Saruri MA, Sorkhabi R, Baraba R. Sedimentary basins of Yemen: their tectonic development and lithostratigraphic cover. Arab J Geosci. 2010;3:515–527.
18. Heikal MTS, Lebda EMM, Orihashi Y, Habtoor A. Petrogenetic evolution of basaltic lavas from Balhaf-Bir Ali Plio-Quaternary volcanic field, Arabia Sea, Republic of Yemen. Arab J Geosci; 2012.
19. Mattash MA, Pinarelli L, Vaselli O, et al. Continental Flood Basalts and Rifting: Geochemistry of Cenozoic Yemen Volcanic Province, Int J Geosci. 2013;4(10):1459-1466.
20. Available:https://www.alsglobal.com/locations/americas/northamerica/canada/britishcolumbia/vancouver-geochemistry-analytical
21. McLennan SM, Murray RW. Geochemistry of sediments. In: Marshall CP, Fairbridge W editors. Geochemistry. Dordrecht: Springer; 1999.
22. Ghandour I, Basaham A, Haredy R, et al. Geochemistry of the Gulf of Aden beach sands, Al-Mukhalla, Yemen: provenance and tectonic setting implications. Acta Geodynamica et Geomaterialia. 2019;16(1):55-69.

23. Ali A, Wagreich M. Geochemistry, environmental and provenance study of the Middle Miocene Leitha limestones (Central Paratethys). Geol Carpath. 2017;68:248-268.
24. El-Anwar AA, Mekky HS, El Rahim AE. Mineralogy, geochemistry, petrography, and depositional environment of Gebel El-Qurn, Early Eocene, West Luxor, South Egypt. Bull Nat Res Centre. 2018;42:7-23.
25. Yano M, Yasukawa K, Nakamura K, et al. Geochemical Features of Redox-Sensitive Trace Metals in Sediments under Oxygen-Depleted Marine Environments. Minerals. 2020;10:1021.
26. Roy S. Environments and processes of manganese deposition. Econ Geol. 1992;87:1218–1236.
27. Schmidt K, Bau M, Hein J, Koschinsky A. Fractionation of the geochemical twins Zr-Hf and Nb-Ta during scavenging from seawater by hydrogenetic ferromanganese crusts. Geochim Cosmochi. Acta. 2014;140:468–487.
28. Nicholson K. Contrasting mineralogical-geochemical signatures of manganese oxides: guides to metallogenesis. Econ Geol. 1992;87:1253–1264.
29. Schultz HD. Quantification of early diagenesis: dissolved constituents in pore water and signals in the solid phase. In: Schultz HD, Zabel M, editors. Marine Geochemistry, 2nd ed. Heidelberg: Springer. 2006:75–77.
30. Bonatti E, Kraemer T, Rydell H. Classification and genesis of submarine ironmanganese deposits. In: Horn D editor. Ferromanganese Deposits on the Ocean Floor. Washington: Natl Sci Found. 1972:149–165.
31. Zhang KJ, et al. Geochemistry of limestones deposited in various plate tectonic settings. Earth-Sci Rev; 2017
32. Jemmali N, Souissi F, Carranza EJM, Henchiri M. Geochemistry of Triassic Carbonates: Exploration Guide to Pb–Zn Mineralization in North Tunisia. Res Geol. 2016;66: 335-350.
33. Holster, W.T. Evaluation of the application of rare-earth elements to paleoceanography. Palaeogeogr. Palaeoclimatol. Palaeoecol. 1997;132:309–323.
34. Pourret, O., Davranche, M., Gruau, G., Dia, A. New insights into cerium anomalies in organic-rich alkaline waters. Chem. Geol. 2008;251:120–127.

Peer-review history:
The peer review history for this paper can be accessed here:
http://www.sdiarticle4.com/review-history/69750